Passive permeability controls synthesis for the allelochemical sorgoleone in sorghum root exudate

Saad Raza,[†] Troy H. Sievertsen,[‡] Sakiko Okumoto,[¶] and Josh V. Vermaas[*,†,‡]

[†]*Plant Research Laboratory, College of Natural Science, Michigan State University, East Lansing MI 48824*

[‡]*Department Of Biochemistry and Molecular Biology, College of Natural Science, Michigan State University, East Lansing MI 48824*

[¶]*Department Of Soil and Crop Sciences, College of Agriculture and Life Sciences, Texas A&M University, College Station TX 77843*

E-mail: vermaasj@msu.edu

Phone: +1 (517) 884-6937

Abstract

Competition for soil nutrients and water with other plants foster competition within the biosphere for access to these limited resources. The roots for the common grain sorghum produce multiple small molecules that are released via root exudates into the soil to compete with other plants. Sorgoleone is one such compound, which suppresses weed growth near sorghum by acting as a quinone analog and interferes with photosynthesis. Since sorghum also grows photosynthetically, and may be susceptible to sorgoleone action if present in tissues above ground, it is essential for sorgoleone to be excreted efficiently. However, since the P450 enzymes that synthesize sorgoleone are intracellular, the release mechanism for sorgoleone remain unclear. In this study, we

conducted an *in silico* assessment for sorgoleone and its precursors to passively permeate biological membranes. To facilitate accurate simulation, CHARMM parameters were newly optimized for sorgoleone and its precursors. These parameters were used to conduct one microsecond of unbiased molecular dynamics simulations to compare the permeability of sorgoleone with its precursors molecules. We find that interleaflet transfer is maximized for sorgoleone, suggesting that the precursor molecules may remain in the same leaflet for access by biosynthetic P450 enzymes. Since no sorgoleone was extracted during unbiased simulations, we compute a permeability coefficient using the inhomogeneous solubility diffusion model. The requisite free energy and diffusivity profiles for sorgleone through a sorghum plasma membrane model were determined through Replica Exchange Umbrella Sampling (REUS) simulations. The REUS calculations highlight that any soluble sorgleone would quickly insert into a lipid bilayer, and would readily transit. When sorgleone forms aggregates in root exudate as indicated by our equilibrium simulations, aggregate formation would lower the effective concentration in aqueous solution, creating a concentration gradient that would facilitate passive transport. This suggests that sorgoleone synthesis occurs within sorghum root cells and that sorgoleone is exuded by permeating through the cell membrane without the need for a transport protein.

Introduction

Sorghum is a cereal grain grown on a global scale for its diverse utility as an alternative energy resource, food for livestock and people, and for its ability to survive and flourish in harsh conditions.[1,2] One of the factors contributing to the adaptability of sorghum to harsh environment is an allelochemical compound called sorgoleone. Sorgoleone is released as exudate from the roots of the sorghum plant and it inhibits photosynthesis in germinating seedlings.[3–7] Sorgoleone is strongly hydrophobic, so it is sorbed and persists in the soil and persists in the soil[8,9] which causes soil sickness and diminishes growth of other neighboring plants,[10–13] while also reducing soil nitrification.[14,15] Sorgoleone suppresses growth for many plants, but is most commonly active on small-seeded plants including *Abutilon theophrasti*, *Datura stramonium*, *Amaranthus retroflexus*, *Setaria viridis*, *Digitaria sanguinalis*, and *Echinochloa crusgalli*.[12,16–20]

Sorgoleone biosynthesis was discovered using retrobiosynthetic NMR analysis of sorghum root exudate.[21,22] The polyketide synthase involved in sorgoleone synthesis is in a different cellular compartment than the fatty acid synthase.[21] The sorghum root hairs have all the necessary components to synthesize sorgoleone, and do create exudate droplets that are approximately 50% sorgeleone by weight.[3,9] The exudate droplets may accumulate to 20 micrograms in size per miligram of dry root weight in laboratory conditions.[3]

This inhibition may be necessary to avoid autotoxicity,[24] as the chemical structure for sorgoleone (Fig. 1) is analogous to ubiquinone, a ubiquitous electron carrier in bacterial photosynthesis and mitochondria. Crucially, sorgoleone closely mimics intermediates in the ubiquinone biosynthesis pathway, replacing a methyl group with a hydroxyl group when compared with demethoxyquinone, the substrate for Coq7 in yeast, UbiF in *E. coli*,[25] and potentially homologs of At1g24340 in plants.[26] Thus, sorgoleone may inhibit ubiquinone biosynthesis, or directly inhibit photosynthetic or mitochondrial proteins by mimicking ubiquinone or potentially plastoquinone directly. Regardless, photosynthetic activity in the presence of sorgoleone is diminished,[3–5] as is mitochondrial function,[27] providing a competitive ad-

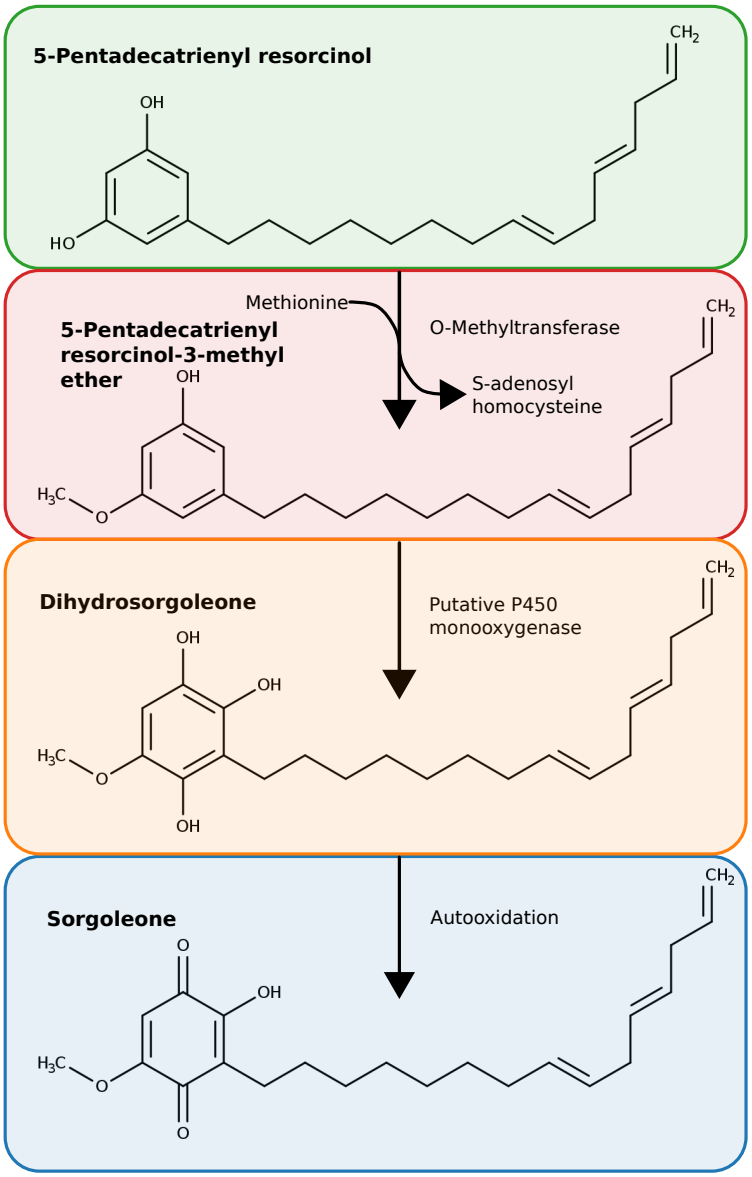

Figure 1: Chemical structures of sorgoleone and it precursors selected for the current permeability study, together with the last steps of the biosynthesis pathway, adapted from.[23] The putative synthesis pathway begins from 5-pentadecatrienyl resorcinol, which is converted by o-methyltransferase to 5-pentadecatrienyl resorcinol-3-methyl ether to dihydrosorgoleone via a undetermined P450 enzyme, before autooxidizing to sorgoleone. The chemical structure for sorgoleone is very similar to that of quinones used as electron carriers within the light reactions of photosynthesis.

vantage if sorghum can efficiently export sorgoleone while reducing its own susceptibility to this chemical. Thus, determining membrane permeation and compartmentalization of sorgolenone and its precursors is essential to understanding the growth-defense tradeoff for sorghum to synthesize sorgoleone while not poisoning itself.

In the sorgoleone synthesis pathway (Fig. 1),[23] a specialized polyketide synthase called acyl-resorcinol synthase forms the aromatic ring and links this ring to the C-16 acyl tail which results into a compound called 5-pentadecatrienyl resorcinol.[21] Then 5-pentadecatrienyl resorcinol with the help of an O-Methyltransferase is converted into 5-Pentadecatrienyl resorcinol-3-methyl ether, which is then converted to dihydrosorgoleone through a putative P450 monooxygenase[21] (Fig. 1). Acyl-resorcinol synthase enzymes are intracellular, and are localized to the membrane surface.[28,29] O-Methyltransferase and a putative P450 monooxygenase are localized to the cytosol, but were not tested for membrane binding.[29,30] Localization of sorgoleone synthesis pathway enzymes to the cytosol suggests that sorgoleone is manufactured on the plasma membrane or the endoplasmic reticulum, even if localization of O-Methyltransferase and the putative P450 monooxygenase are not well established. Thus, the current study focuses on the passive permeation of sorgoleone and the final three precursors (5-pentadecatrienyl resorcinol, 5-Pentadecatrienyl resorcinol-3-methyl ether, dihydrosorgoleone, Figure 1) through the sorghum plasma membrane.

Our tools for this study are classical molecular dynamics (MD) simulations, which have a long history of providing mechanistic insight into passive transport processes.[31–33] The simulations entail two parts, with unbiased simulations providing a qualitative description for the membrane insertion process, as well as statistics on interleaflet exchange for these compounds. As extraction from the lipid bilayer for these compounds is not spontaneous on typical MD-timescales, replica exchange umbrella sampling (REUS) was used to sample along both the extraction and leaflet traversal reaction coordinates to yield energy barriers and diffusivity profiles along these pathways.[34,35] When coupled to the inhomogeneous solubility diffusion model,[32,33,36] this yields a quantitative permeability coefficient for these small

molecules across the sorghum membrane. We find that sorgoleone is the most permeable compound of the four tested (Fig 1). Furthermore, sorgoleone and its precursors may form aggregates in solution at high concentrations, analogous to a proto-droplet of root exudate.

Methods

The overall workflow for the research is to build a representative sorghum plasma membrane model, add in our compounds of interest (Fig. 1), and carry out classical MD simulations either with or without applied biases to sample the passive permeation process. Good membrane building tools exist to build mixed membrane systems,[37–39] and permeation quantification methods from simulation are well established.[33,36] However, as these small molecules are not commonly simulated, we first need to discuss their parameterization in detail.

Sorgoleone and Dihydoxysorgoleone Parameterization

Accurate classical simulations depend on parameterizing the underlying energy landscape into the applied forcefield. We use the CHARMM force field due to its well established performance for membrane systems,[40–42] which features a simplified forcefield that depends only on coordinates and pre-defined interactions and atomtypes to determine potential energy.

$$
\begin{aligned}
U_{total} =& U_{non-bonded} + U_{bonded} \\
U_{total} =& (U_{VDW} + U_{electrostrostatic})_{non-bonded} + (U_{bonds} + U_{angles} + U_{dihedrals} + U_{impropers})_{bonded} \\
U_{total} =& \left(\left[\sum_{i,j} \epsilon_{i,j} \left(\left(\frac{R_{i,j}^{min}}{r_{i,j}} \right)^{12} - 2 \left(\frac{R_{i,j}^{min}}{r_{i,j}} \right)^{6} \right) \right] + \left[\frac{q_i q_j}{4\pi\epsilon_0 r_{ij}} \right] \right) + \\
& \left(\left[\sum_i k_i \Big(b_i - b_0 \Big)^2 \right] + \left[\sum_i k_i \Big(a_i - a_0 \Big)^2 + k_i^{UB} \Big(ub_i - ub_0 \Big)^2 \right] + \right. \\
& \left. \left[\sum_i k_i \Big(1 + \cos(n_i \chi_i + \delta_i) \Big) \right] + \left[\sum_i k_i \Big(\chi_i - \chi_0 \Big)^2 \right] \right)
\end{aligned} \tag{1}
$$

From the potential energy function in Eq. 1,[43–45] we can determine the forces applied to each atom by taking the gradient of the potential energy function at the atomic position. Forces are contributed both through pair wise non-bonded interactions for all atom pairs i and j (red text in Eq. 1) and multibody terms that describe the bonded interaction for bonded atoms in the system (blue text in Eq. 1). Note that Eq. 1 features many elements that are parameterized not to vary with atomic position, such as equilibrium bond lengths (b_0), partial atomic charges (q) and other similar terms that constitute the force field. These parameters are available for many small molecules using the CHARMM general force field,[43,46] which uses quantum mechanical target data for related compounds to determine by analogy parameters for similar molecules. When analogous topologies have not been previously parameterized in the general force field, optimization of the interaction parameters encoded by Eq. 1 is required.

The molecular structure of sorgoleone was retrieved from PubChem,[47] checking the geometry to determine the correct conformer. Structurally, sorgoleone has a polar head group and lipophilic tail similar to the lipids in bilayer. The sorgoleone tail is highly analogous to lipid acyl tails, and thus could be treated by analogy. However, the quninone head and the various electron donating and withdrawing groups mandated careful parameterization. To reduce the computational cost of parameterization, only the quinone headgroup was further optimized, with structure split at the second carbon of the tail as shown in Figure S1. The sorgoleone head group was mutated into dihydroxysorgoleone (Figure S2), 5-Pentadecatrienyl resorcinol-3-methyl ether and 5-Pentadecatrienyl resorcinol precursor head group according to the structure given in Figure 1 through the structure editing tools built into UCSF-Chimera.[48]

Parameters for the four quinone head groups were generated using the standard CHARMM parameterization procedures, implemented within the FFparam tool kit.[49] Quantum mechanical (QM) potential energies for multiple conformations were calculated using Gaussian 16 C.01,[50] which was considered a target for the fitting of MM parameters. Consistent with

typical parameterization recommendations from other groups,[49,51] QM geometry optimization for the head group was performed using the MP2/6-31G* basis set. Partial charge optimization was carried out using the quantum energies for water interaction at the HF/6-31G* level of theory. Optimizations of the bonding parameters were done at MP2/6-31G* level of theory. The QM scans for restrained dihedrals in the head group were restricted to 120° with 60° in each direction of the equilibrium angle with 10° steps.

QM target data generated with above mentioned protocol was imported into FFparam to build MM system to optimize the parameters in Eq. 1.[44] Monte Carlo simulated annealing (MCSA) algorithm[49] implemented in FFparam was used to optimize partial charges, and further manual fine-tuning was done to minimize the error gap between QM and MM results. Autofitting of the bonded parameters to minimize differences between QM and MM energies for equivalent geometries was performed using LSFITPAR,[52] together with manual refinements to guide the minimization procedure towards values consistent with the rest of the CHARMM force field. The head group and tail were combined using the CHARMM patching machinery built into `psfgen` within VMD.[53]

Molecular System Assembly

Molecular environment of the lipid bilayer for sorghum membrane was generated using CHARMM-GUI (Figure 2).[37–39] The composition of the head group of the sorghum membrane was a 35:25:23:12:6:2:2 ratio for phosphatidyl choline (PC), digalactosyl diacylglycerol (DGDG), monogalactosyl diacylglycerol (MGDG), phosphatidyl ethanolamine (PE), sterols, phosphatidyl glycerol (PG), phosphatidyl serine (PS), respectively, based on available lipidomics data.[54,55] The fully detailed composition is presented in Table 1. Four total simulation systems were built, one for each of the molecules of interest. In each case, the initial systems were built by adding twenty copies of each molecule into the system. Initially, ten were placed above the membrane, and ten were placed at the bottom using the TopoTools module within VMD.[53,56] Each sorgoleone precursor was placed at 35 Å away

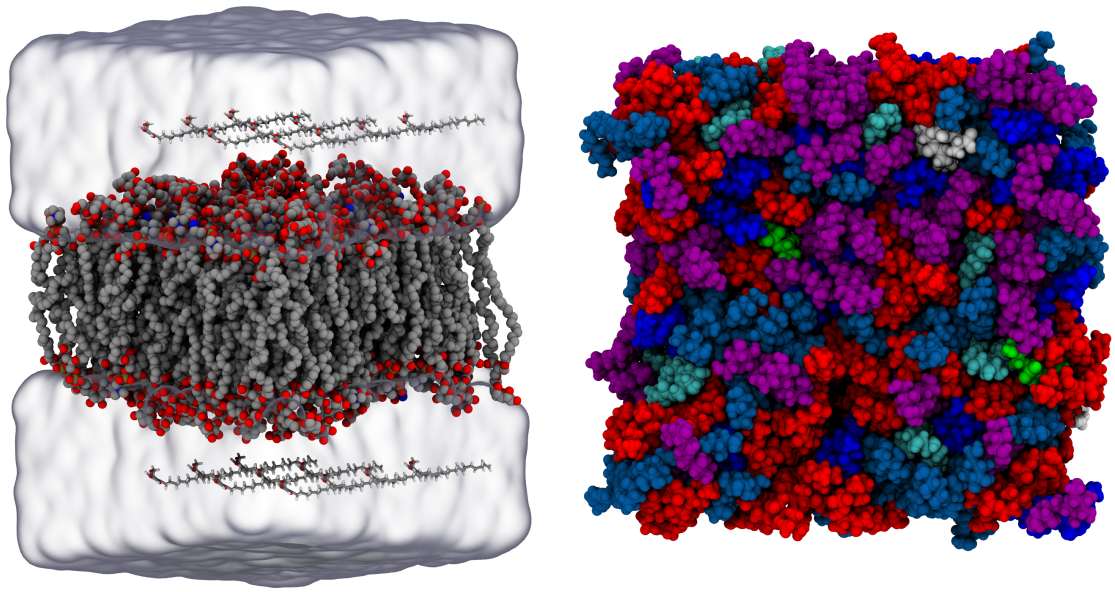

Figure 2: A representative starting configuration to begin simulation the starting distribution of sorgoleone around the bilayer. The glass bubble representation shows the solution area. The sorgoleone is represented in licorice representation above and below the membrane, and bilayer heavy atoms are portrayed as beads, with the hydrogens omitted for visual clarity. (Right) A top view for the headgroup distribution within the sorghum. Each headgroup in this view has a unique color, red for PC, blue for PE, green for PG, white for PS, purple for DGDG, light blue for MGDG and cyan for sterols.

from the center of membrane on both ends. The system was then solvated in a TIP3 water model box through `solvate` plugin with VMD.[53,57] Counterions were added to neutralize the system and add 150 nM concentration of NaCl using the `autionize` module in VMD.[53] The dimension of the simulation box for all systems was 80 Å in the x and y axes parallel to the membrane surface and 115 Å along the z-axis perpendicular to the membrane surface. When complete, these systems were approximately 67,000 atoms in size.

Simulation Protocol

Multiple molecular dynamics protocols were used in this study to assess the behavior of sorgoleone and its precursors:

1. Unbiased simulations studied the equilibrium behavior for the compounds within a sorghum membrane model.

2. REUS simulations are used to quantify the free energy and diffusivity profiles for the small molecules along three independent but complimentary reaction coordinates to capture permeation and transport phenomena:

   (a) Interleaflet exchange for the sorgoleone-related compounds, where the quinone headgroups are tracked relative to the center of the lipid bilayer.

   (b) The desorption from membrane to absorption into water for the sorgoleone-related compounds. In this instance, the process is controlled by biasing the number of atomic contacts between the entire sorgoleone molecule and the lipid bilayer.

   (c) The desorption from membrane to absorption into an organic phase for the sorgoleone-related compounds. This process is steered by the contact difference between sorgoleone molecule and lipid bilayer and the other between sorgoleone and organic phase.

Each of the simulation protocols is explained in the following subsections.

Table 1: Head group and tail composition of one leaflet of sorghum bilayer used for equilibration and steered molecular dynamics (SMD) simulation.

		Sorghum	
Lipid Head Groups	Tails	Equilibration	SMD
PC	16:0-18:1	3	1
	16:0-18:2	12	4
	16:0-18:3	8	3
	18:0-18:2	1	-
	18:2-18:2	8	3
	18:2-18:3	3	1
PE	16:0-18:1	1	-
	16:0-18:2	6	2
	16:0-18:3	2	1
	18:2-18:2	2	1
	18:2-18:3	1	-
PS	16:0-18:2	1	-
	20:1-20:1	1	-
PG	16:0-16:0	1	-
	16:0-18:2	1	-
DGDG	16:0-18:1	2	1
	16:0-18:2	11	4
	16:0-18:3	7	3
	18:0-18:2	1	-
	16:0-20:4	1	-
	18:2-18:3	1	-
	18:3-18:3	2	1
MGDG	16:0-18:1	3	1
	16:0-18:2	6	2
	16:0-18:3	3	1
	18:0-18:2	1	-
	16:0-20:4	2	1
	18:2-18:3	2	1
	18:3-18:3	6	3
Sterols		6	2

Unbiased Simulation

Classical molecular dynamics can provide insights into the mechanics of permeability at the atomic level by measuring the flow of molecules in the membrane. Simulations were carried out using the CHARMM36 force field for lipids and small molecules,[40,43,58] which was supplemented by our reparameterization as stated above and provided in the Supporting Information.A combination of NAMD 2.14 and NAMD 3.0a9 was used as the molecular dynamics engine.[59] Minimization was performed with NAMD 2.14, and unbiased simulations were performed using the GPU-resident integrator on NAMD 3.0a9 to maximize performance.[59] A Langevin barostat was used to maintain pressure at 1 atm.[60] Temperature was controlled using the Langevin thermostat at 298 K with 1 ps^{-1} damping. Hydrogen bonds were handled with SETTLE algorithm to enable 2 fs timesteps.[61] Long-range electrostatic interactions were calculated with particle mesh Ewald (PME) grid with 1.2 Å.[62,63] Energy minimization of the system was initially performed using the 1000 steps of conjugate gradient in NAMD.[64] The system was then allowed to equilibrate for 50 ps in NPT ensemble using 5 Å margin to allow the box to adjust after any distortion from minimization prior to transitioning to the GPU-resident integrator. Simulations in the production NPT ensemble were run for 1 μs with default margin to maximize performance.

Replica Exchange Umbrella Sampling Simulations

Sorgoleone and its precursors were observed to spontaneously integrate into the membrane from aqueous solution in equilibrium simulation. However, interleaflet transitions were sporadic, so transition counting methods to assess permeation were not feasible.[36] REUS was performed to evenly sample along the adsorption/desorption pathway as well as the interleaflet transition pathway.[65] These are each sampled with independent reaction coordinates, implemented using the colvars module[66] within NAMD.[59] The observed barrier to interleaflet transitions are breaking interactions between the quinone headgroup and the surrounding environment featuring lipid headgroups and water. The hydrophobic sorgleone tails follow

the headgroup. Thus, measuring progress for the interleaflet transition based strictly on the position of the quinone headgroup is appropriate. However, the primary barrier along the adsorption and desorption pathway are hydrophobic contacts between the lipid tails.[67,68] Along this pathway, the key metric to track are contacts between the molecule of interest and the surrounding hydrophobic environment, with zero contacts representing the desorbed state. This split reaction coordinate is analogous to simulations performed for fatty acid permeation,[69] and eliminates ambiguities that might arise from two orientations or conformations for a molecule sharing a center of mass (Figure S6).

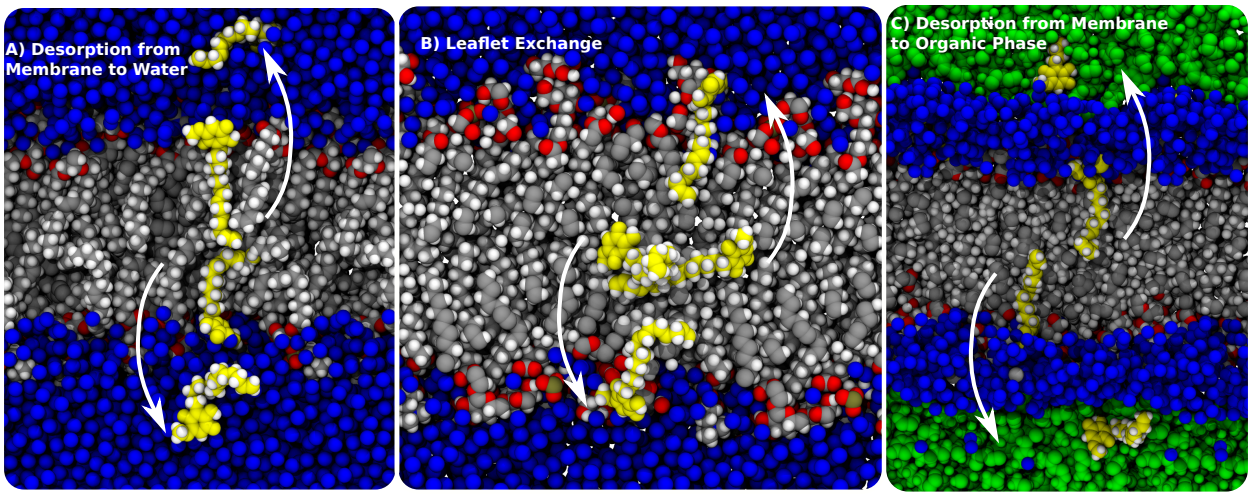

Figure 3: Example states of first and last replica for three different REUS calculation. These REUS calculation are for sorgoleone desorption from membrane to absorption in water (A), leaflet exchange of sorgoleone within a membrane (B) and sorgoleone desorption from membrane to absorption in an organic phase phase of sorgoleone (C). Each representation is detailing the relative positioning of the sorgoleone (yellow) compared with the membrane (atomically colored spheres), water (blue), and the organic phase of sorgoleone (green). Hydrogen atoms of water are omitted for clarity.

To prepare the simulations for desorption from the membrane to water, we reduce the equilibrium simulation systems from Table 1 to only carry a two copies of sorgoleone or its precursors in the membrane, on in each leaflet. These new systems were simulated for 200 ns to allow sorgoleone or its precurors to insert, as was seen in equilibrium simulations. These pre-equilibrated systems were the basis for the REUS campaign. Exchanges between adjacent replicas during REUS were carried out every picosecond, with exchange ratios near

the 20% optimum.[70]

To sample interleaflet exchange (Figure 3B), the sorgoleone precursors were pulled via steered molecular dynamics (SMD) to prepare the REUS ladder over 5 ns using a 5 kcal mol^{-1} Å^{-2} force constant, with each precursor sampling from the membrane midplane to the membrane edge, 25 Å away. The membrane midplane was determined by selecting the C16 atoms of the lipid acyl chains. All non hydrogen atoms on sorgoleone and its precursors along with the even carbon atoms on the acyl chain were used in colvars for REUS. The REUS simulation used 48 equi-spaced replicas taken from this initial SMD trajectory to cover this span with 99 ns of sampling in each umbrella, or 4.7μs in aggregate per compound.

To sample desorption from membrane to absorption in to water (Figure 3A), we used the following definition to measure a coordination number, which we use to measure contacts:

$$C^{ij} = \sum_{i \in ligand} \sum_{j \in membrane} \frac{1 - \left(\frac{|r_i - r_j|}{4\text{Å}}\right)^6}{1 - \left(\frac{|r_i - r_j|}{4\text{Å}}\right)^{12}} \tag{2}$$

Here C^{ij} is the matrix element quantifying the contacts between sorgoleone and membrane, where i and j represent indices of the pairs of atoms used for the calculation of the contact number, while r_i and r_j are the coordinates of the atoms. For performance reasons, the contact number was only quantified between non hydrogen atoms on sorgoleone and its precursor and the heavy atoms in the head group and even carbons atoms of acyl tail of lipids. The colvar module[66] was used to determine the contact number from Equation 2 to use as the starting position for the SMD, which was obtained from the pre-equilibrated system. The SMD simulation reduced the contact number from 180 (membrane bound compound) to 0 (compound in solution) by pulling with 0.1 kcal mol^{-1} contact^{-2} force constant over 5 ns. REUS simulations were performed using 64 replicas with force constant of 0.1 kcal mol^{-1} contact^{-2} to restraint each of the sorgoleone and it's precursors on equally displaced umbrellas from contact number 180 to 0. Each replicate was run 73.5 ns, or 4.7 μs in aggregate sampling per compound.

To sample sorgoleone desorption from membrane and absorption into an organic sorgoleone droplet, we used a slighlty different simulation system modeled on prior work around fatty acid and terpene extraction (Figure 3C).[69,71] We built a block of organic phase using the GROMACS insert-molecules module, and briefly equilibrated it to achieve a well-packed organic phase positioned above the membrane. Bilayer was retained along the water within 8 Å of bilayer from the previous SMD system. Block of organic phase was placed on top and bottom of the retained system. To simulate desorption from membrane and absorption into an organic phase, we took the difference between the molecule contacts with the membrane and organic phase components, using the same formulation as Eq. 2.

$$C^{ij} = \left(\sum_{i \in ligand} \sum_{j \in membrane} \frac{1 - \left(\frac{|r_i - r_j|}{6\text{Å}} \right)^4}{1 - \left(\frac{|r_i - r_j|}{6\text{Å}} \right)^{12}} \right) - \left(\sum_{i \in ligand} \sum_{j \in organicphase} \frac{1 - \left(\frac{|r_i - r_j|}{6\text{Å}} \right)^4}{1 - \left(\frac{|r_i - r_j|}{6\text{Å}} \right)^{12}} \right) \quad (3)$$

Eq. 3 was used then to drive the diffusion of sorgoleone from membrane to organic phase. As before, the contacts number were calculated using non hydrogen atoms on sorgoleone and the heavy atoms in the head group and even carbons atoms of acyl tail of lipids. Equation 3 definition was applied using colvar module[66] and utilized in SMD to move the sorgoleone molecule from membrane into the organic phase from 400 to -1000 contact number. Here 400 value represent sorgoleone in the membrane and the -1000 value represents sorgoleone complete absorption in the organic phase. In SMD simulation the sorgoleone was pulled with 0.01 kcal mol^{-1} contact^{-2} force constant over 15 ns. REUS simulations were performed using 96 replicas with force constant of 0.005 kcal mol^{-1} contact^{-2} to restraint sorgoleone on equally displace umbrellas from contact number -1000 to 400. Each replicate was run for 60 ns or 5.7μs in aggregate sampling.

Analysis

Structure files and MD simulation trajectories were visualized and analyzed using Python-enabled VMD 1.9.4a55 and Chimera.[48,53] Python enabled VMD provides an interface to

apply the numpy numerical library and plotting tools like matplotlib.[72,73]

To compute permeation coefficients, we rely on the inhomogeneous solubility diffusion model.[32,74,75] To apply this method, free energy and diffusivity profiles are calculated along the representative reaction coordinate, often the membrane normal,[33,55,71,76] and combined via the following equation:

$$Pm = \left[\int_{\xi_l}^{\xi_u} \frac{exp\big(\Delta G(\xi)\beta\big)}{D(\xi)} d\xi \right]^{-1} \tag{4}$$

Based on Eq. 4, the permeability coefficient Pm is dependent on free energy profile (ΔG) along with local diffusion (D) integrated along a reaction coordinate ξ between upper (ξ_u) and lower (ξ_l) bound of permeation endpoints. The complementary datapoint is the partition coefficient (P), frequently reported in logarithmic scale, which relates the favorability between a molecule in the membrane and aqueous solution.

$$\log P = \frac{G_{aq} - G_{membrane}}{RT \ln 10} = \frac{\Delta G_{partition}}{RT \ln 10} = \frac{[membrane]}{[aqueous]} \tag{5}$$

Positive logP values indicate that the molecule will accumulate in the membrane.

REUS simulations were analyzed to determine both a free energy profile and a diffusivity profile for each molecule along both reaction coordinates to feed into Eq. 4. The free energy profiles were determined with a modified version of Bayesian Weighted Histogram Analysis Method (BayesWHAM),[77] which uses Gibbs sampling of the known Dirichlet prior[78] to rapidly assess uncertainty. Diffusion profile for Eq. 4 is calculated from variance and autocorrelation time of the biased motion along the reaction coordinate.[79] The autocorrelation time itself is estimated from an exponential fit over the short time where a trajectory remains within a single umbrella. This approach is less sensitive to the harmonic restraint force than alternative calculation approaches,[80] and is independent of momentum removal around restarts.[81]

To compute an overall permeability coefficient for the full process, we leverage the fact

that the integral in Eq. 4 can be split into multiple components. The overall resistance to permeation is additive across the individual steps such as adsorption, leaflet exchange, and desorption in the total permeation process. This follows the prior precedents in other permeation studies for complex membranes or compounds.[55,69,76,82] To create a connected free energy profile that spans the full space, we take advantage of our trajectories and free energies to reweight our sampling from one reaction coordinate to the other. From our free energy profiles, we can obtain a probability distribution in both distance space ($P_{distance}$) and coordination number space ($P_{contact}$). From our trajectories, we can determine the probability of existing at a specific coordination number given a distance ($P_{contacts|distance}$) or the opposite ($P_{distance|contacts}$). Then Bayes rule allows us to create a transformed probability, which can be converted back to free energy after reweighting.

$$P_{distance} = \frac{P_{(distance|contacts)} P_{(contacts)}}{P_{(contacts|distance)}} \tag{6}$$

Results

Measuring passive permeability of sorgoleone and its precursors through a sorghum plasma membrane model is carried out systematically through a MD simulation campaign. The methodological starting point was the optimization of molecular parameters for sorgoleone and its precursors. Optimized parameters enable us to use these molecules to predict their localization in a membranous environment through microsecond-scale unbiased MD simulation. However, since sampling from classical MD simulation is limited to local free-energy minima and does not explore the entire energy landscape, we also use REUS techniques to estimate the permeability coefficient.

Sorgoleone and Dihydrosorgoleone Parameterization

Detailed discussion of the methodology and results around parameterization are provided in the Supporting Information. Some of the key significant details will be highlighted here specific to parameter optimization. Bonds and angle parameters were not parameterized as they showed overlap with quantum mechanics results (Figure S2). Optimizing the water interactions around sorgoleone yielded an improved fit, with a RMSE that is only one quarter of the error from the initial values provided by CGenFF (Table S1). The distribution of charges on dihydrosorgoleone was relatively complex, in comparison to sorgoleone. Quantum mechanics results suggested a relatively high interaction energy for one of hydroxyl and adjacent water molecules. To satisfy this energy, a compromise must be made in the water interaction with lone pair of hydroxy oxygen (Table S2). Similar to this case, the lone pair on the adjacent ether oxygen interaction energy is excluded to better fit other interaction energies.

After the optimization of charges, dihedral potential energy functions were fit based on QM energy scans. The dihedrals suggested for optimization by CGenFF penalty scores were all linked through the ring of sorgoleone and dihydrosorgoleone (Figures S3 and S4). These dihedrals are naturally coupled together, and are fit through a collective set of QM energy scans. In the case of sorgoleone, the CGenFF parameter overestimates the barrier around the energy minima in the scan (Figure S3). By contrast, the initial CGenFF parameters for hydroxysorgoleone underestimated the barrier heights (Figure S4). After optimization, the discrepancy between the energy scans was significantly reduced, representing an accurate model for these crucial compounds.

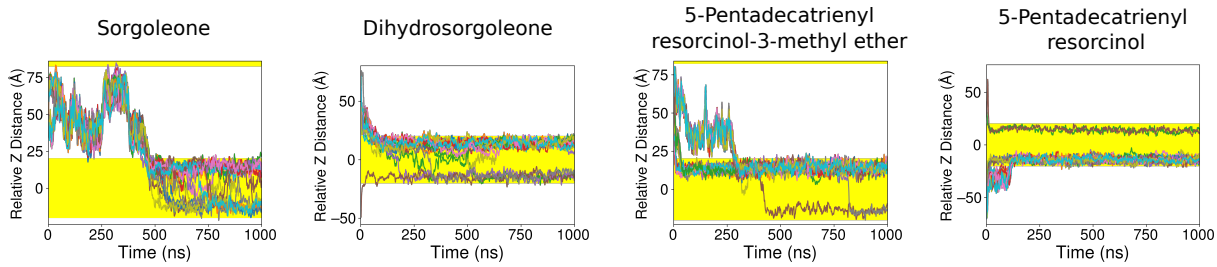

Figure 4: Position trace for each molecule, measuring the relative position of the geometric center for the quinone rings and the membrane midplane during equilibrium simulation. Since each system had 20 molecules (Fig. 2), there are 20 lines with different colors representing the trace for an individual molecule. The trace has been unwrapped to eliminate discontinuities around the membrane normal dimension. The yellow shaded area represents the membrane extent, while the uncolored background represents the solvent.

Permeation for Sorgoleone and its Precursor into Sorghum Membrane

After parameterization, we are specifically interested in tracking permeation for sorgoleone or its precursors across plant plasma membranes. For species that permeate quickly, equilibrium simulation is sufficient to track membrane crossing events, where a small molecule passes from one leaflet to the next, analogous to prior studies.[55,71,76,82] Since sorgoleone and the other molecules share a large hydrophobic lipid tail, we would expect each of the molecules to quickly insert into the bilayer. We can quantify this motion by plotting the relative z-distance between the membrane and the quinone headgroup for each of the individual molecules placed in the simulation (Fig. 4). Different molecules insert into the membrane at different rates. The initial equal spacing between molecules quickly breaks down, as sorgoleone and the other molecules will aggregate in solution prior to permeating into the membrane bulk. Once associated to the membrane, the compounds dissociate from each other and separate from one another.

The dissociation after membrane association can be observed from the intermolecular contacts decreasing upon membrane association. The intermolecular contacts between individual small molecules decrease as soon as the contact between those molecules and the

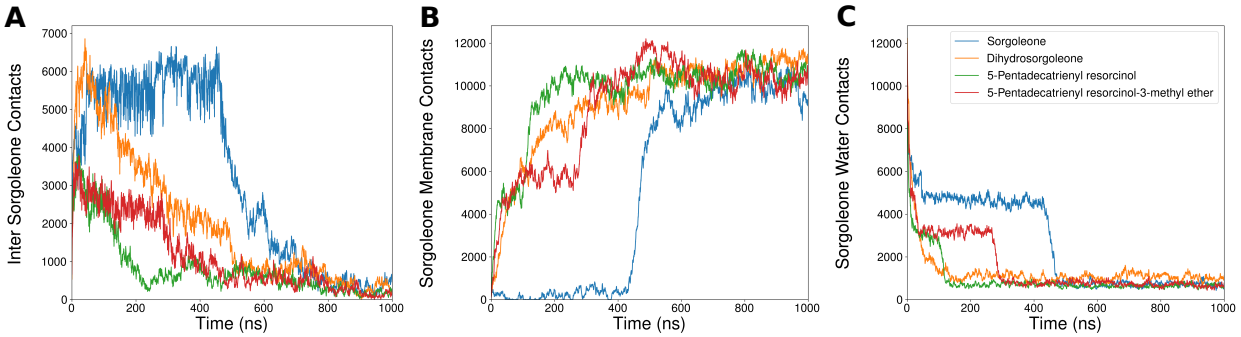

Figure 5: Quantification for plot for (A) inter sorgoleone contacts, (B) membrane-sorgoleone contacts and (C) water-sorgoleone contacts, with the timeseries for different sorgoleone and its precursor in different colors. The inter sorgoleone contact sum is determined by first computing the distance between sorgoleone heavy atoms that are not members of the same residue. Sorgoleone-membrane contact sum is determined by first computing the distance between sorgoleone and membrane heavy atoms. Sorgoleone-water contact sum is determined by first computing the distance between sorgoleone heavy atoms and water oxygen atoms. The distances are then weighted the distance-weighted contact function from Eq. 2, and the individual C values are summed together to yield the total contact number.

membrane increases (Fig. 5A and 5B). Once these molecules are inside the membrane, the molecules will gradually spread out, and eschew contact with the water. Surprisingly, this suggests that the head group of sorgoleone and its precursors are buried slightly deeper in the membrane than a typical lipid headgroup, and has relatively little interaction with water (Fig. 5C).

Circling back to the association process, our sorgoleone aggregate was the slowest to penetrate the membrane, when compared with other small molecules along the synthesis pathway (Figure 4). While we do not have nearly enough statistics to make definitive conclusions, retarding sorgoleone reentry into the membrane once in root exudates would certainly be useful to minimize autotoxicity, and may require further study. Furthermore, analysis of Figure 4 also demonstrates that sorgoleone, despite having the shortest membrane residence time, switches leaflets most frequently compared with the other precursors. We quantify this movement by counting the number of times the different small molecules switch leaflets during these equilibrium simulations (Table S3). Sorgoleone transits between membrane leaflets more than its precursors by almost an order of magnitude, which would be a positive

indicator for a high potential flux out of the cell.

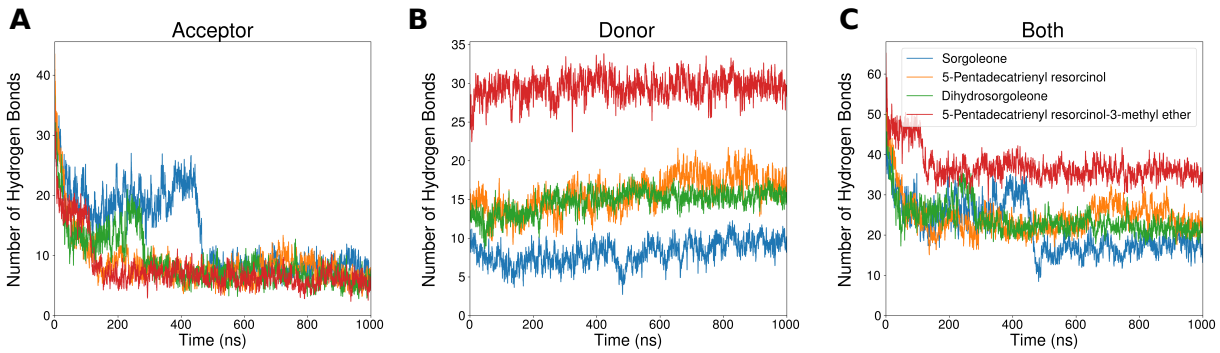

Figure 6: Quantification plot for hydrogen bonds where (A) sorgoleone and its precursors are forming the hydrogen bonds as hydrogen bond acceptors or (B) as hydrogen bond donors. The sum of both acceptor and donor interactions are given in panel (C).

Chemically speaking, the increased mobility for sorgoleone appears tied to its propensity to hydrogen bond differently than the other compounds in the study. Quantifying hydrogen bonds where our molecules of interest are either a donor or acceptor (Figure 6), we find that the number of times that the molecules act as hydrogen bond acceptors is relatively consistent across molecules (Figure 6A), despite the varied functional groups presence and quantity in the precursors (Figure 1). However, sorgoleone is the worst hydrogen bond donor (Figure 6B), as its only hydroxyl group is adjacent to the hydrophobic tail, relatively inaccessible to other potential hydrogen bond partners. Since phospholipid head groups have more hydrogen bond acceptors than donors, a poor proton donor like sorgoleone will have fewer interactions with the headgroup. With fewer interactions tethering the compound to a single leaflet, interleaflet transfer for sorgoleone is accelerated.

Headgroup interactions with phospholipids lead to a consistent depth distribution for these molecules at around 12-18 Å relative to the membrane center (Fig. S5A). This is comparable to prior simulation studies for ubiquinone,[83,84] where the quinone headgroup is frequently found near the membrane surface. Interestingly, we find that the equilibrium position for the quinone headgroups in our compounds are slightly deeper than in these comparison studies, with the distribution peaking near the membrane carbonyl groups in the acyl tails. Ordinarily, we would anticipate that the additional hydroxyl group relative

to ubiquinone would draw the headgroup closer to the membrane surface, tempered with the removal of the methoxy group in sorgoleone relative to ubiquinone. Methoxy groups draw the quinone towards the membrane surface, possibly due to water interactions with the methoxy oxygen.

In principle, transition events observed in Figure 4 could be used to measure fluxes. However, counting based permeation methods depend on observing crossing events during unbiased simulations, whereas we see very few transition events, creating large uncertainties as to the potential flux within our simulations. Furthermore, we do not see a single case where these small molecules come out of the membrane, as would be expected during the process of forming root exudates. The REUS approach uses biased simulations to circumvent these limitations, and allow for robust permeability estimates.

Sorgoleone Partitioning and Permeability from REUS

Lipids or compounds with long lipophilic tails have heterogeneous tail configurations. A given molecule with long acyl tail may have multiple conformations that resolve to the same center of mass (Fig. S6). This potential to map distinct states to equivalent values for a specific collective variable is a well-known issue in the enhanced sampling literature,[67,85] convolute the interpretation for the center of mass relative to the membrane center for the compounds from Figure 1. As detailed in the methods, our approach to compute the permeability and partitioning behavior for the selected compounds is to split apart the leaflet exchange or membrane crossing step apart from the adsorption and desorption steps, calculating the free energy and diffusivity needed to determine permeability (Fig. 7) in two parts and then merging these elements together to obtain a permeability estimate for sorgoleone and the other related compounds.

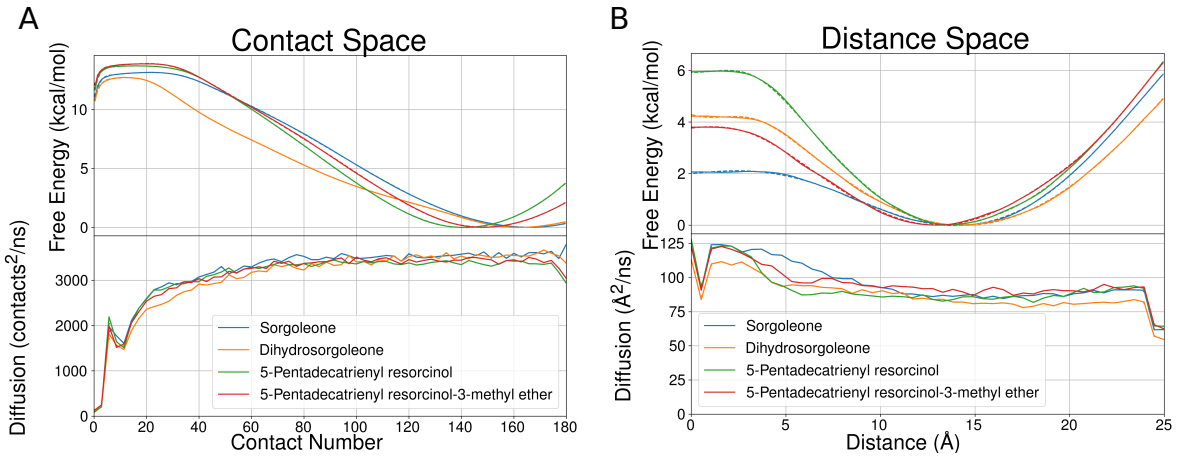

Figure 7: Free energy profile and local diffusivity for sorgoleone and its precursors in contact space (A) and distance space (B). For the free energy profile, the reference point was chosen to be the free energy minima, which at almost right end of the graph in contact space (A) and middle for the distance space (B). In contact space (A) the molecules are pulled outside the membrane which corresponds to left side and pulling outside in distance space (B) is towards the right. Standard errors for the free energy profile are drawn as semitransparent regions, which are rarely visible outside of the main line. Each compound has two lines associated with it, a solid line reflecting the instantaneous best estimate for the quantity of interest and a dashed line indicating the spline fit used to numerically integrate Equation 4 to tabulate permeability coefficients.

REUS for Membrane Adsorption and Desorption

To track adsorption and desorption for sorgoleone from the membrane, we use a collective variable based on coordination number to assess progress. In this instance, zero contacts would represent a desorbed state, where the compound of interest makes no or minimal contact with the membrane. Conversely, the fully membrane embedded state would have a high number of contacts. The free energy profile along this reaction coordinate (Fig. 7A) has a maximum when the compounds are desorbed, which rapidly decreases once the molecules interact with the membrane. This behavior is qualitatively similar to what was observed in equilibrium simulation, that there is a strong driving force for these molecules to remain membrane embedded.

Using REUS calculations, we can quantify this specifically, measuring an energetic difference of ~ 13 kcal/mol between the adsorbed and desorbed states. Previously it has been

reported that phospholipids featuring two acyl chains and thus approximately double the hydrophobic interactions pay a ~ 20 kcal/mol price to desorb,[86] and fatty acid compound with one acyl chain encounter a barrier around ~ 10 kcal/mol.[69] The difference of around 3 kcal/mol in additional cost to desorb a sorgoleone from the membrane may be an effect of membrane composition, or potentially additional hydrophobic bulk offered by the quinone headgroup, as the desorption cost for a lipophillic molecule is driven by hydrophobic bulk.[68] Regardless, much of the cost to desorbing sorgoleone clearly represents the effect of drawing the acyl tails into an aqueous solvent environment.

From the potential energy function (Fig. 7A) we observe that the these molecules encounter no barrier to insert in the membrane. Thus, the partitioning between membrane and solution is effectively only governed by the partition coefficient between membrane and solution. In all cases, the partition coefficients inferred from Fig. 7A are very high, with the estimated concentrations in the membrane 10 billion-fold higher in the membrane versus in solution (Table 2). While passive lipid transport mechanisms reliant on lipid transit through an aqueous environment, these processes are slow.[87,88] Thus, passive processes alone may not be enough to nucleate an extracellular protodroplet of root exudate that would potentially grow as more sorgoleone is produced.

The diffusivity profile for the adsorption and desorption process reveals more about the nature of the reaction coordinate than actual dynamics. Diffusivity along the contact number reaction coordinate is lowest at low coordination number, where relatively large changes in conformation would only minimally change the contact number because of how far it is from the membrane surface. Typical acyl tail dynamics are quite able to change the contact number when the sorgoleone has substantial contacts with the membrane interior, increasing diffusion in these regions.

REUS for Interleaflet Exchange

Both the equilibrium simulation and REUS along the adsorption/desorption pathway for sorgoleone and precursors indicate that these molecules can freely insert into the membrane with no energy barrier. While we did observe membrane crossing events during our equilibrium simulations (Fig. 4, Table S3), the number of events is not statistically significant on their own. Thus, we supplement these simulations with additional REUS simulations to sample along the leaflet exchange coordinate, moving the quinone head group along distance based reaction coordinates from one leaflet of the membrane to another leaflet. Since this reaction coordinate was sampled with two molecules moving to the midplane, creating a symmetric profile, Figure 7B only reports free energies and diffusivities from the membrane midplane at 0 to the outer edge of the membrane at 25 Å.

The energy minimum position for quinone head group of the molecules was around 13-14 Åaway from the center of membrane which lies below the phosphate head group, at approximately the level of the lipid carbonyl groups in the surrounding membrane. This is similar to the position determined from equilibrium simulations (Fig. S5A). As discussed with the equilibrium results, the preferred depth for the quinone headgroup is driven largely by the hydrogen bonds that the quinones make with the surrounding environment. The reduced hydrogen bonding for sorgoleone when compared with its precursors (Fig. 6) manifests in Fig. 7 as the lowest barrier to interleaflet exchange when the compound crosses the membrane midplane. The sorgoleone precursors, by contrast, need to break additional hydrogen bonds, and thus have larger barriers inhibiting the transition between states.

The diffusion profile in Fig. 7B is highly consistent along the leaflet exchange coordinates. Lower diffusivity at around 25 is due to the phase change from membrane to water, while the lowering of diffusivity around 0 is due to jumping from leaflet to another. Through out the leaflet the diffusivity profile remains unchanged if the molecules are inside one leaflet.

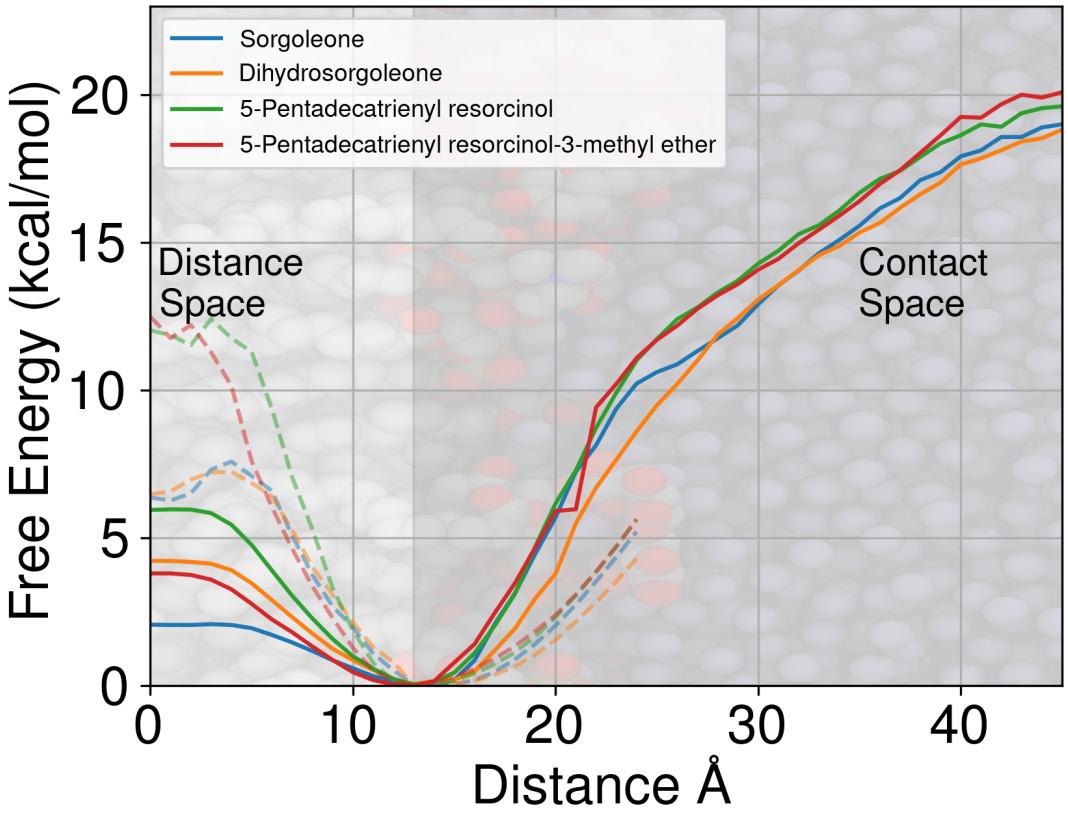

Figure 8: Merged free energy profile from distance and contact space REUS calculation. In this merged representation, the solid line represents the distance free energy profile from Fig. 7B to the left of the minimum, and the free energy profile resulting from transformed probability (Eq. 6) from the contact reaction coordinate sampling (Fig. 7A) into distance space to the right of the minimum. The dashed line represents the converse process, where the distance profile from Fig. 7B is used to the right of the minimum, and the transformed probability profile from the sampling in contact space is used to the left of the profile. As a visual aide, a simplified atomistic representation of the respective components is used as a background, with water oxygens and lipid heavy atoms following a standard color scheme (gray for carbons, red for oxygens in lipids, blue for the oxygen in water, and yellow for phosphorus).

Determining Partitioning and Permeability Coefficients

Figure 7 computes the individual steps needed for passive permeation, from adsorption, crossing, to extraction back into aqueous solution. However, the units are clearly different, and it can be unclear when integrating Eq. 4 how to handle these mixed units to determine permeability coefficients. By reweighting our free energy profiles, we can place both sets of calculations into the same context, using the joint probability within our REUS calculations (Fig. S7) to apply Bayes law (Eq. 6) to binned state probabilities derived from the free energy profile in Fig. 7A. The resulting reweighted free energy profile (Fig. S8) can be plotted on the same reaction coordinate as the interleaflet exchange process, resulting in Fig. 8.

The contact-derived profile in distance space is consistently higher in free energy, highlighting the peril of measuring progress along the wrong reaction coordinate. Rarely sampled regions in space, such as when the quinone headgroup is far away from the membrane surface, will have very high free energies calculated from the joint probability density. Thus the real take-away is not the 20 kcal mol^{-1} free energy estimate for pulling a sorgoleone molecule out of the membrane, as we believe that the contact number-based value of 13-14 kcal mol^{-1} from Fig. 7A is likely more accurate, but that desorption processes are likely to be rate limiting given the large free energy change.

Table 2: Partition (P) and Permeability (Pm_e) coefficient for sorgoleone in sorghum membrane. The partitioning is based on difference in free energy for sorgoleone and its precursors in membrane and water (Eq). Permeability is decomposed into crossing permeability (Pm_c), calculated via a distance REUS calculation and extraction permeability (Pm_{ex}), calculated via a contacts-based REUS sampling approach. These permeabilities are calculated as discussed in methods by equation 4. The effective permeability coefficient (Pm_e) is calculated as $\log\left[Pm_e\right] = \log P + \log_{10}\left[\left(Pm_c^{-1} + 2Pm_{ex}^{-1}\right)^{-1}\right]$, and represents the permeability coefficient for compounds from aqueous solution to aqueous solution through the membrane.

Compound Name	$\log P$	$\log_{10}\left[Pm_e\,(cms^{-1})\right]$	$\log_{10}\left[Pm_c\,(cms^{-1})\right]$	$\log_{10}\left[Pm_{ex}\,(cms^{-1})\right]$
Sorgoleone	9.6	1.7	1.0	-7.7
Dihydrosorgoleone	9.3	1.3	-0.4	-7.7
5-Pentadecatrienyl resorcinol	10.1	1.3	-1.6	-8.4
5-Pentadecatrienyl resorcinol-3-methyl ether	10.2	2.3	-0.0	-7.6

Connecting the independent free energy minima together to construct Figure 8 provides

the natural breakpoints needed to integrate Eq. 4, splitting the overall permeation process into crossing and adsorption/desorption components. Together with the partition coefficient, these elements together can be combined following prior literature to obtain an effective permeability coefficient (Pm_e, Table 2)[69,71,76,82] that quantifies the flux across a membrane from the inside to the outside of a cell given a concentration gradient across the membrane. Within Table 2, we see that the effective permeability coefficient is very high, consistent with a regime where passive transport processes would dominate,[76] without the need for a transport protein to facilitate sorgoleone permeation.

However, unlike previous studies for lignin where the small molecules are reasonably water soluble,[76] the partition coefficients inferred from our simulations are larger and positive, indicating that sorgoleone or its precursors are over a billion-fold enriched in the membrane relative to aqueous solution (Table 2). From the permeability calculation, we observe that the rate limiting step from passive permeation of the sorgoleone and its precursor molecules is the membrane extraction step, which is over a million times slower than exchange between leaflets.

REUS for Diffusion into an Organic Phase

From our analysis of leaflet exchange REUS, sorgoleone is the product that diffuses between membrane leaflets most readily. However, the energy barrier for crossing the membrane to an extracellular aqueous environment seems to be more than $10\,\mathrm{kcal\,mol^{-1}}$. This high barrier would make it difficult for sorgoleone molecules diffuse out into the extracellular aqueous environment. Upon looking at the unbiased simulation we observed that sorgoleone forms an aggregated mass to insert into the membrane, and that perhaps sorgoleone spontaneously desorbs from the membrane to join the larger aggregate, or at least would do so far more favorably than directly to aqueous solution.

The system with a sorgoleone organic layer using the collective variable described in Equation 3 is designed to test this hypothesis, with the free energy diagram shown in Fig. 9.

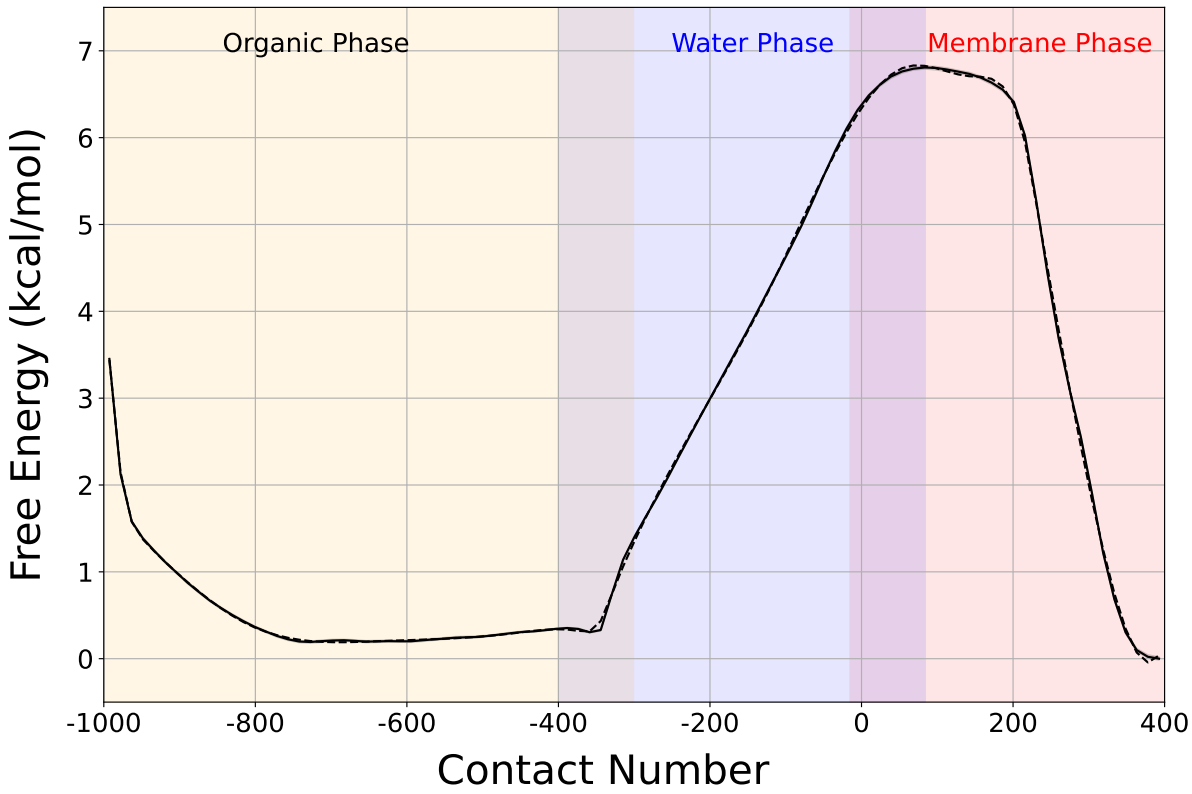

Figure 9: Free energy profile for sorgoleone for desoprtion from membrane and absorption into an organic phase. For the free energy profile, the reference point was chosen to be the free energy minima, which is at almost right end of the graph when sorgoleone is in the membrane. The sorgoleone are pulled out of the membrane into the organic phase (left side). Standard errors for the free energy profile are drawn as semitransparent regions, which are rarely visible outside of the main line. Sorgoleone has two lines associated with it, a solid line reflecting the instantaneous best estimate for the quantity of interest and a dashed line indicating the spline fit.

The free energy profile in Fig. 9 from our REUS calculation for absorption into an organic phase suggest that there is a ¡ 0.5 kcal mol^{-1} difference between the membrane bound state and organic phase. Moreover, the barrier to desorbing from the membrane is smaller in Fig. 9 than it was in the equivalent desorption profile in Fig. 7A, suggesting that perhaps sorgoleone could span the space between membrane and the organic phase above it.

The surprisingly similar energetics for sorgoleone in both the membrane and an organic phase, separated by a significant barrier in the aqueous phase, highlight how droplets and membranes may co-exist in a natural system. If an active transport system of some sort could drive sorgoleone from the membrane to a nascent droplet, that droplet may continue to grow without reabsorbing under specific conditions. In developing test simulations to compute Fig. 9, if the aqueous layer is thinner than 8 Å, the organic phase and the membrane would readily fuse. Glycans decorating the membrane lipids may thus facilitate efficient sorgoleone compartmentalization into droplets than can be released into the soil.

Discussion

Following Table 2 and observing the behavior of sorgoleone in equilibrium simulation, we can start to make some mechanistic hypotheses for how sorgoleone is synthesized and exported. The long hydrophobic tails present in sorgoleone precursors mean that the molecules will be present in the membrane. Thus, it stands to reason that the synthesis enzymes carrying out the reactions put forward in Fig. 1 should all be membrane associated, even if that association is at the membrane periphery. This is consistent with the cytosolic localization of many of the pathway enzymes,[23] which could interact with intracellular precursors at the membrane interface. The order of reactions appears optimized to retain sorgoleone precursors on one side of the membrane, as the resorcinol derivatives cross the membrane slower than sorgoleone or dihydrosorgoleone. From an export perspective, the molecule with the closest transport rate to sorgoleone is dihydrosoroleone, which may simply be oxidized in the extracellular

space if it is released before oxidation. *In planta*, maintaining biosynthetic precursors on one side of the membrane would be an attractive strategy to improve synthetic efficiency, as only half as many molecules would need to be made to reach a certain concentration on one side of the membrane, increasing enzymatic efficiency. However, as the concentration rises, it is clear that interleaflet exchange would occur over the hours and days in a plant lifetime, and so we would expect to find some concentration for all of the compounds of interest in the outer leaflet within sorghum root hairs.

This raises a natural question of how sorghum itself is able to avoid being poisoned by sorgoleone, as sorgoleone is so permeable across lipid bilayers. In part, the high barrier to desorb from a lipid bilayer may contribute. An intracellular concentration of sorgoleone within a root hair cell of 1 nM would correspond to a 1-10 M concentration in the membrane, based on the logP value of around 10 and the concentration definition from Eq. 5. This 1 nM concentration is well below the inhibitory concentration for sorgoleone *in vitro*.[27] Thus, the intracellular concentration would be smaller, and so long as sorgoleone production is isolated to the root hairs, the flux to other tissues would be limited by the number of membranes that would need to be traversed and the capacity for these other membranes to soak up large quantities of sorgoleone.

We can work out an example from the typical Fickian flux equation:

$$J = PmA\Delta C \tag{7}$$

where the molecular flux (J) is proportional to the permeability coefficient, the contact surface area (A), and the change in concentration between the adjacent compartments (Δ C). If there were a thousand membrane traversals between a root hair with our high 1 nM intracellular concentration and a photosynthetic cell that initially has no sorgoleone in it and may have some slow degradation process to metabolize sorgoleone, the eventual solution is for a steady state to be reached. The concentration difference between individual cells

would only be on the pM scale, as the overall ΔC between the start and end-points would be evenly divided across all the membranes separating compartments that need to be traversed. Assuming 100 μm of contact area between cells, the steady state flux would be 5×10^{-20} moles of sorgoleone per second, or about 30,000 molecules per second. Naturally, as the initial intracellular concentration goes down, this steady state flux would as well. Crucially, we are assuming that the concentration differences across the plant are governed primarily by membrane traversals, rather than other potential transport mechanisms through the xylem or phloem or junctions between plant cells.

For a typical plant, 1000 cells in the previous example would be on the centimeter length-scale. Thus, as plants grow, the ability for sorgoleone to reach photosynthetic tissues will diminish as more membranes would need to be crossed, shrinking the gradient that is driving sorgoleone flux. This finding is the mechanism underpinning why sorgoleone is most effective on shorter weeds and less effective on established plants,[3] as a greater fraction of the plant cells would be accessible to inhibitory concentrations of sorgoleone. Since sorghum grows to be relatively tall, sorgoleone's impact on its native host would be minimal, so long as the plant localizes sorgoleone synthesis to the roots far away from photosynthetic tissues, and controls the timing to only enable exudate production after the plant reaches a specific height. The sorghum would then only need a relatively feeble detoxification mechanism to deal with the sorgoleone that travels up the plant and still grow unimpeded.

The other major question is how droplets of root exudate form in the first place. Imagining a scenario where there is initially no root exudate droplet present, the concentration for sorgoleone in the extracellular space will be equal to the concentration inside the root hair cell where sorgoleone is synthesized. While we observe that sorgoleone will aggregate quickly in solution (Fig. 5), and that the energetic difference between a blob of sorgoleone in solution and sorgoleone in the membrane is small (Fig. 9), we also see that sorgoleone droplets may reinsert into the membrane. Naturally, reinsertion needs to be avoided somehow, otherwise sorgoleone will never make it into the soil and carry out its allelochemical function.

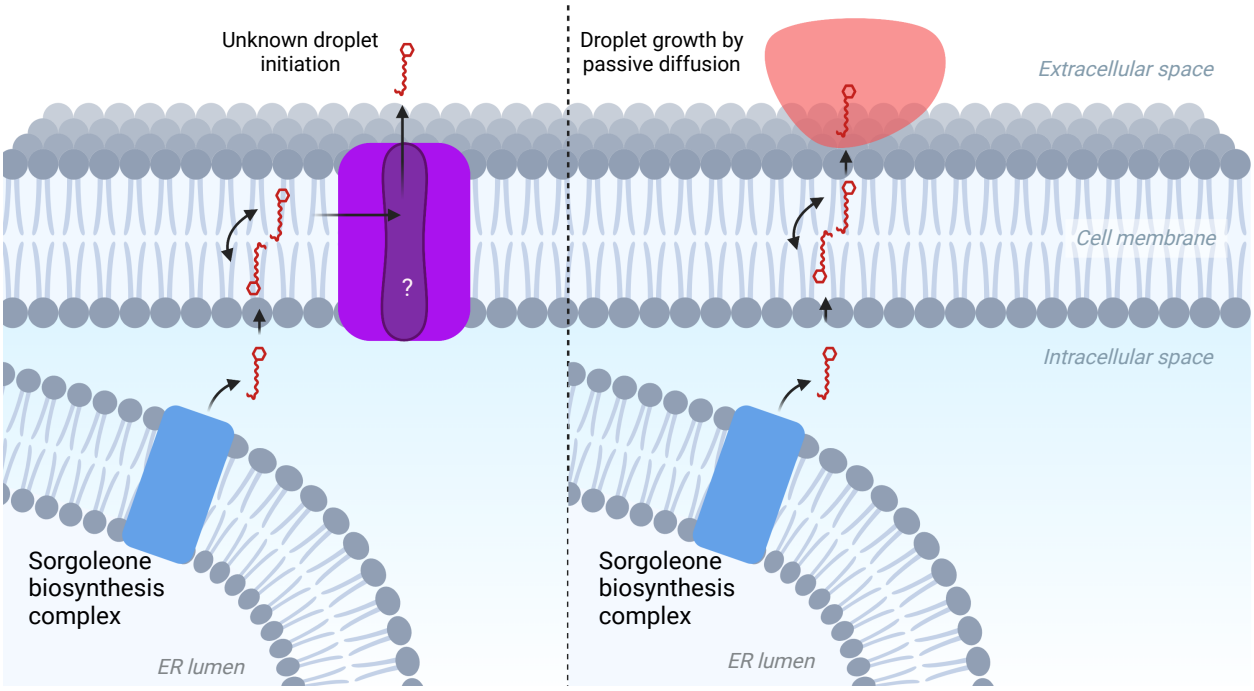

Figure 10: Proposed schematic for sorgoleone secretion. While synthesized in the ER, sorgoleone would readily transport by vesicle trafficking or passive diffusion to the plasma membrane, where a droplet is initiated by an unknown mechanism. Once a droplet is initiated, as it is in the right panel, passive diffusion could feasibly feed continued aggregation into a larger droplet.

One can imagine that large droplets may have sufficient cohesive forces or that specific lipid moieties on the outer surface of sorghum root hairs may prevent reinsertion. Alternatively, specially shaped proteins or other structures, such as perhaps a lipophilic spire, may facilitate exudate droplet formation and act to prevent reinsertion (Fig. 10). Yet another possibility is that while single sorgoleone molecules can traverse the plant cell wall in the root tips, the droplet would be prevented from returning to the plasma membrane. These mechanistic hypotheses are testable, but go beyond the scope of the current study. As we have shown (Fig. 9), if a sufficiently large droplet could be established by one of these unknown mechanisms, it is possible that the free energy change for desorption from the membrane to the exudate phase is reduced substantially (Fig. 10). The reduction in free energy when desorbing into an organic phase is similar to what was observed for desorbing terpenes from the membrane to an organic phase in prior computational studies.[71] Just as in microbial engineering studies where products must be exported non-destructively, and so non-polar solvents are frequently used for extraction, sorgoleone manufactured in the cell could be spontaneously exported into organic droplets, without needing to invoke a transport protein, even if active droplet initiation cannot be ruled out (Fig. 10). The droplets themselves would be carried through the soil, or potentially breakup when they hit a soil particle, and would diffuse in the local soil environment.

The growth rate for individual droplets could be quite high. Based on the permeability coefficients from Table 2, small concentration gradients will quickly be dissipated by molecules following the gradient through diffusion. Once sorgoleone is incorporated into a droplet, forming a distinct phase independent from the aqueous phase, the concentration in water will be very low again. Realizing that flux is directly proportional to the concentration difference (Eq. 7), the high flux will be maintained. *In vivo*, the droplets will diffuse into the surrounding environment, with the concentration limited primarily by degradation by microbes or the environment.

Conclusion

Through equilibrium and non-equilibrium molecular dynamics simulations, we have explored the membrane interaction for sorgoleone and its precursors, including reparameterization for these compounds where appropriate. We find that these compounds will spontaneously insert into lipid membranes in molecular simulation timescales with high affinity, and may also interchange between leaflets. Sorgoleone has the most rapid interleaflet exchange rate, and its precursors may remain on one side of the membrane during the synthesis process. When membrane bound, the quinone headgroup for sorgoleone is near the membrane surface, at approximately the level of membrane carbonyl groups, while its acyl tail is in the membrane core.

From biased simulation, we determine the permeability coefficient for these compounds across the sorghum plasma membrane. The molecules are determined to be highly permeable, with bilayer transit for limited primarily by desorption from the membrane. Desorption from the membrane can be facilitated by large droplets of an organic phase. While permeable, concentrations within the host are limited by the number of membrane jumps between root cells that generate sorgoleone and photosynthetic cells sensitive to sorgoleone, mitigating autotoxicity. Thus, we find that sorgoleone likely is transported passively across membranes and through plants, rather than being actively exported to maintain low sorgoleone concentrations inside a sorghum cell.

Supporting Information Available

The Supporting Information (SI) primarily features additional a detailed description of the parameterization process for the sorgoleone and dihydroxysorgoleone considered here, as well includes quantification for the number of crossing events observed during simulation. It has the steps and outputs for the conversion of contact space reaction space to distance based reaction space. All input scripts to build and run molecular simulations are made publicly

available on Zenodo.[89]

Acknowledgement

We acknowledge support from the Institute for Cyber Enabled Research (ICER) at MSU, which provided the computing resources utilized for this project. This work used the Extreme Science and Engineering Discovery Environment (XSEDE), which is supported by National Science Foundation grant number ACI-1548562[90] (project number TG-BIO210040). Figure 10 created with BioRender.com.

Declaration of generative AI and AI-assisted technologies in the writing process

During the preparation of this work the authors used Writefull in order to make suggestions to improve the flow and grammar of the manuscript. After using this tool/service, the authors reviewed and edited the content as needed and take full responsibility for the content of the publication.

References

(1) Tari, I.; Laskay, G.; Takács, Z.; Poór, P. Response of sorghum to abiotic stresses: A review. *Journal of agronomy and crop science* **2013**, *199*, 264–274.

(2) Hossain, M. S.; Islam, M. N.; Rahman, M. M.; Mostofa, M. G.; Khan, M. A. R. Sorghum: A prospective crop for climatic vulnerability, food and nutritional security. *Journal of Agriculture and Food Research* **2022**, 100300.

(3) Dayan, F. E.; Howell, J.; Weidenhamer, J. D. Dynamic root exudation of sorgoleone

and its in planta mechanism of action. *Journal of Experimental Botany* **2009**, *60*, 2107–2117.

(4) Dayan, F. E.; Rimando, A. M.; Pan, Z.; Baerson, S. R.; Gimsing, A. L.; Duke, S. O. Sorgoleone. *Phytochemistry* **2010**, *71*, 1032–1039.

(5) Dayan, F. E.; Duke, S. O. *Plant-derived natural products*; Springer, 2009; pp 361–384.

(6) Einhellig, F. A.; Rasmussen, J. A.; Hejl, A. M.; Souza, I. F. Effects of root exudate sorgoleone on photosynthesis. *Journal of chemical ecology* **1993**, *19*, 369–375.

(7) Gonzalez, V. M.; Kazimir, J.; Nimbal, C.; Weston, L. A.; Cheniae, G. Inhibition of a photosystem II electron transfer reaction by the natural product sorgoleone. *Journal of Agricultural and food Chemistry* **1997**, *45*, 1415–1421.

(8) Demuner, A. J.; Barbosa, L. C.; Chinelatto Jr, L. S.; Reis, C.; Silva, A. A. Sorption and persistence of sorgoleone in red-yellow latosol. *Quimica Nova* **2005**, *28*, 451–455.

(9) Besançon, T. E.; Dayan, F. E.; Gannon, T. W.; Everman, W. J. Conservation and Divergence in Sorgoleone Production of Sorghum Species. *J. environ. qual.* **2020**, *49*, 368–377.

(10) Breazeale, J. Injurious after-effects of sorghum. *Agronomy journal* **1924**,

(11) Einhellig, F. A.; Rasmussen, J. A. Prior cropping with grain sorghum inhibits weeds. *Journal of Chemical Ecology* **1989**, *15*, 951–960.

(12) Forney, D. R.; Foy, C. L.; Wolf, D. D. Weed suppression in no-till alfalfa (Medicago sativa) by prior cropping of summer-annual forage grasses. *Weed Science* **1985**, *33*, 490–497.

(13) Putnam, A. R.; DeFrank, J.; Barnes, J. P. Exploitation of allelopathy for weed control in annual and perennial cropping systems. *Journal of Chemical Ecology* **1983**, *9*, 1001–1010.

(14) Gao, X.; Uno, K.; Sarr, P. S.; Yoshihashi, T.; Zhu, Y.; Subbarao, G. V. High-Sorgoleone Producing Sorghum Genetic Stocks Suppress Soil Nitrification and N2O Emissions Better than Low-Sorgoleone Producing Genetic Stocks. *Plant Soil* **2022**, *477*, 793–805.

(15) Sarr, P. S.; Nakamura, S.; Ando, Y.; Iwasaki, S.; Subbarao, G. V. Sorgoleone Production Enhances Mycorrhizal Association and Reduces Soil Nitrification in Sorghum. *Rhizosphere* **2021**, *17*, 100283.

(16) Netzly, D. H.; Butler, L. G. Roots of sorghum exude hydrophobic droplets containing biologically active components 1. *Crop Science* **1986**, *26*, 775–778.

(17) Barbosa, L. C. d. A.; Ferreira, M. L.; Demuner, A. J.; Silva, A. A. d.; Pereira, R. d. C. Preparation and phytotoxicity of sorgoleone analogues. *Quimica Nova* **2001**, *24*, 751–755.

(18) Souza, C. N. d.; Souza, I.; Pasqual, M. Extração e ação de sorgoleone sobre o crescimento de plantas. *Ciência e Agrotecnologia* **1996**, *23*.

(19) Einhellig, F. A.; Souza, I. F. Phytotoxicity of sorgoleone found in grain sorghum root exudates. *Journal of Chemical Ecology* **1992**, *18*, 1–11.

(20) Panasiuk, O.; Bills, D. D.; Leather, G. R. Allelopathic influence ofSorghum bicolor on weeds during germination and early development of seedlings. *Journal of chemical ecology* **1986**, *12*, 1533–1543.

(21) Dayan, F. E.; Kagan, I. A.; Rimando, A. M. Elucidation of the biosynthetic pathway of the allelochemical sorgoleone using retrobiosynthetic NMR analysis. *Journal of Biological Chemistry* **2003**, *278*, 28607–28611.

(22) Fate, G. D.; Lynn, D. G. Xenognosin methylation is critical in defining the chemical potential gradient that regulates the spatial distribution in Striga pathogenesis. *Journal of the American Chemical Society* **1996**, *118*, 11369–11376.

(23) Maharjan, B.; Vitha, S.; Okumoto, S. Developmental Regulation and Physical Interaction among Enzymes Involved in Sorgoleone Biosynthesis. *The Plant Journal* **2023**, *115*, 820–832.

(24) Dayan, F. E. Factors modulating the levels of the allelochemical sorgoleone in Sorghum bicolor. *Planta* **2006**, *224*, 339–346.

(25) Pelosi, L.; Ducluzeau, A.-L.; Loiseau, L.; Barras, F.; Schneider, D.; Junier, I.; Pierrel, F. Evolution of ubiquinone biosynthesis: multiple proteobacterial enzymes with various regioselectivities to catalyze three contiguous aromatic hydroxylation reactions. *MSystems* **2016**, *1*, e00091–16.

(26) Latimer, S.; Keene, S. A.; Stutts, L. R.; Berger, A.; Bernert, A. C.; Soubeyrand, E.; Wright, J.; Clarke, C. F.; Block, A. K.; Colquhoun, T. A.; others A dedicated flavin-dependent monooxygenase catalyzes the hydroxylation of demethoxyubiquinone into ubiquinone (coenzyme Q) in Arabidopsis. *Journal of Biological Chemistry* **2021**, *297*.

(27) Rasmussen, J. A.; Hejl, A. M.; Einhellig, F. A.; Thomas, J. A. Sorgoleone from Root Exudate Inhibits Mitochondrial Functions. *J Chem Ecol* **1992**, *18*, 197–207.

(28) Monroe, S. H.; Johnson, M. A. Membrane-bound O-methyltransferase of Douglas-fir callus. *Phytochemistry* **1984**, *23*, 1541–1543.

(29) Baerson, S. R.; Dayan, F. E.; Rimando, A. M.; Nanayakkara, N. D.; Liu, C.-J.; Schroder, J.; Fishbein, M.; Pan, Z.; Kagan, I. A.; Pratt, L. H.; others A functional genomics investigation of allelochemical biosynthesis in Sorghum bicolor root hairs. *Journal of Biological Chemistry* **2008**, *283*, 3231–3247.

(30) Neve, E. P.; Ingelman-Sundberg, M. Intracellular transport and localization of microsomal cytochrome P450. *Analytical and bioanalytical chemistry* **2008**, *392*, 1075–1084.

(31) Krämer, A.; Ghysels, A.; Wang, E.; Venable, R. M.; Klauda, J. B.; Brooks, B. R.; Pastor, R. W. Membrane permeability of small molecules from unbiased molecular dynamics simulations. *The Journal of Chemical Physics* **2020**, *153*, 124107.

(32) Marrink, S. J.; Berendsen, H. J. Permeation process of small molecules across lipid membranes studied by molecular dynamics simulations. *The Journal of Physical Chemistry* **1996**, *100*, 16729–16738.

(33) Lee, C. T.; Comer, J.; Herndon, C.; Leung, N.; Pavlova, A.; Swift, R. V.; Tung, C.; Rowley, C. N.; Amaro, R. E.; Chipot, C.; others Simulation-based approaches for determining membrane permeability of small compounds. *Journal of chemical information and modeling* **2016**, *56*, 721–733.

(34) Oshima, H.; Re, S.; Sugita, Y. Replica-exchange umbrella sampling combined with Gaussian accelerated molecular dynamics for free-energy calculation of biomolecules. *Journal of Chemical Theory and Computation* **2019**, *15*, 5199–5208.

(35) Yoda, T.; Sugita, Y.; Okamoto, Y. Comparisons of force fields for proteins by generalized-ensemble simulations. *Chemical Physics Letters* **2004**, *386*, 460–467.

(36) Venable, R. M.; Krämer, A.; Pastor, R. W. Molecular dynamics simulations of membrane permeability. *Chemical reviews* **2019**, *119*, 5954–5997.

(37) Jo, S.; Kim, T.; Iyer, V. G.; Im, W. CHARMM-GUI: a web-based graphical user interface for CHARMM. *Journal of computational chemistry* **2008**, *29*, 1859–1865.

(38) Wu, E. L.; Cheng, X.; Jo, S.; Rui, H.; Song, K. C.; Dávila-Contreras, E. M.; Qi, Y.; Lee, J.; Monje-Galvan, V.; Venable, R. M.; others CHARMM-GUI membrane builder toward realistic biological membrane simulations. 2014.

(39) Lee, J.; Patel, D. S.; Ståhle, J.; Park, S.-J.; Kern, N. R.; Kim, S.; Lee, J.; Cheng, X.; Valvano, M. A.; Holst, O.; others CHARMM-GUI membrane builder for complex bi-

ological membrane simulations with glycolipids and lipoglycans. *Journal of chemical theory and computation* **2018**, *15*, 775–786.

(40) Klauda, J. B.; Venable, R. M.; Freites, J. A.; O'Connor, J. W.; Tobias, D. J.; Mondragon-Ramirez, C.; Vorobyov, I.; MacKerell Jr, A. D.; Pastor, R. W. Update of the CHARMM all-atom additive force field for lipids: validation on six lipid types. *The journal of physical chemistry B* **2010**, *114*, 7830–7843.

(41) Klauda, J. B. Considerations of recent all-atom lipid force field development. *The Journal of Physical Chemistry B* **2021**, *125*, 5676–5682.

(42) Sajadi, F.; Rowley, C. N. Simulations of lipid bilayers using the CHARMM36 force field with the TIP3P-FB and TIP4P-FB water models. *PeerJ* **2018**, *6*, e5472.

(43) Vanommeslaeghe, K.; Hatcher, E.; Acharya, C.; Kundu, S.; Zhong, S.; Shim, J.; Darian, E.; Guvench, O.; Lopes, P.; Vorobyov, I.; others CHARMM general force field: A force field for drug-like molecules compatible with the CHARMM all-atom additive biological force fields. *Journal of computational chemistry* **2010**, *31*, 671–690.

(44) Brooks, B. R.; Brooks III, C. L.; Mackerell Jr, A. D.; Nilsson, L.; Petrella, R. J.; Roux, B.; Won, Y.; Archontis, G.; Bartels, C.; Boresch, S.; others CHARMM: the biomolecular simulation program. *Journal of computational chemistry* **2009**, *30*, 1545–1614.

(45) MacKerell Jr, A. D. Empirical force fields for biological macromolecules: overview and issues. *Journal of computational chemistry* **2004**, *25*, 1584–1604.

(46) Vanommeslaeghe, K.; MacKerell, A. D. Automation of the CHARMM General Force Field (CGenFF) I: Bond Perception and Atom Typing. *J. Chem. Inf. Model.* **2012**, *52*, 3144–3154.

(47) Kim, S.; Chen, J.; Cheng, T.; Gindulyte, A.; He, J.; He, S.; Li, Q.; Shoemaker, B. A.; Thiessen, P. A.; Yu, B.; others PubChem in 2021: new data content and improved web interfaces. *Nucleic acids research* **2021**, *49*, D1388–D1395.

(48) Pettersen, E. F.; Goddard, T. D.; Huang, C. C.; Couch, G. S.; Greenblatt, D. M.; Meng, E. C.; Ferrin, T. E. UCSF Chimera—a visualization system for exploratory research and analysis. *Journal of computational chemistry* **2004**, *25*, 1605–1612.

(49) Kumar, A.; Yoluk, O.; MacKerell Jr, A. D. FFParam: Standalone package for CHARMM additive and Drude polarizable force field parametrization of small molecules. *Journal of computational chemistry* **2020**, *41*, 958–970.

(50) Frisch, M. J. et al. Gaussian˜16 Revision C.01. 2016; Gaussian Inc. Wallingford CT.

(51) Mayne, C. G.; Saam, J.; Schulten, K.; Tajkhorshid, E.; Gumbart, J. C. Rapid parameterization of small molecules using the force field toolkit. *Journal of computational chemistry* **2013**, *34*, 2757–2770.

(52) Vanommeslaeghe, K.; Yang, M.; MacKerell Jr, A. D. Robustness in the fitting of molecular mechanics parameters. *Journal of computational chemistry* **2015**, *36*, 1083–1101.

(53) Humphrey, W.; Dalke, A.; Schulten, K. VMD: visual molecular dynamics. *Journal of molecular graphics* **1996**, *14*, 33–38.

(54) Laursen, T.; Borch, J.; Knudsen, C.; Bavishi, K.; Torta, F.; Martens, H. J.; Silvestro, D.; Hatzakis, N. S.; Wenk, M. R.; Dafforn, T. R.; others Characterization of a dynamic metabolon producing the defense compound dhurrin in sorghum. *Science* **2016**, *354*, 890–893.

(55) Raza, S.; Miller, M.; Hamberger, B.; Vermaas, J. V. Plant Terpenoid Permeability through Biological Membranes Explored via Molecular Simulations. *The Journal of Physical Chemistry B* **2023**, *127*, 1144–1157.

(56) Kohlmeyer, A.; Vermaas, J. TopoTools. 2017.

(57) Jorgensen, W. L.; Chandrasekhar, J.; Madura, J. D.; Impey, R. W.; Klein, M. L. Comparison of simple potential functions for simulating liquid water. *The Journal of chemical physics* **1983**, *79*, 926–935.

(58) Lee, S.; Tran, A.; Allsopp, M.; Lim, J. B.; Hénin, J.; Klauda, J. B. CHARMM36 united atom chain model for lipids and surfactants. *The journal of physical chemistry B* **2014**, *118*, 547–556.

(59) Phillips, J. C.; Hardy, D. J.; Maia, J. D.; Stone, J. E.; Ribeiro, J. V.; Bernardi, R. C.; Buch, R.; Fiorin, G.; Hénin, J.; Jiang, W.; others Scalable molecular dynamics on CPU and GPU architectures with NAMD. *The Journal of chemical physics* **2020**, *153*, 044130.

(60) Feller, S. E.; Zhang, Y.; Pastor, R. W.; Brooks, B. R. Constant pressure molecular dynamics simulation: the Langevin piston method. *The Journal of chemical physics* **1995**, *103*, 4613–4621.

(61) Miyamoto, S.; Kollman, P. A. Settle: An analytical version of the SHAKE and RATTLE algorithm for rigid water models. *Journal of computational chemistry* **1992**, *13*, 952–962.

(62) Darden, T.; York, D.; Pedersen, L. Particle mesh Ewald: An N log (N) method for Ewald sums in large systems. *The Journal of chemical physics* **1993**, *98*, 10089–10092.

(63) Essmann, U.; Perera, L.; Berkowitz, M. L.; Darden, T.; Lee, H.; Pedersen, L. G. A smooth particle mesh Ewald method. *The Journal of chemical physics* **1995**, *103*, 8577–8593.

(64) Fletcher, R. *Numerical analysis*; Springer, 1976; pp 73–89.

(65) Sugita, Y.; Kitao, A.; Okamoto, Y. Multidimensional replica-exchange method for free-energy calculations. *The Journal of Chemical Physics* **2000**, *113*, 6042–6051.

(66) Fiorin, G.; Klein, M. L.; Hénin, J. Using collective variables to drive molecular dynamics simulations. *Molecular Physics* **2013**, *111*, 3345–3362.

(67) Rogers, J. R.; Geissler, P. L. Breakage of hydrophobic contacts limits the rate of passive lipid exchange between membranes. *The Journal of Physical Chemistry B* **2020**, *124*, 5884–5898.

(68) Rogers, J. R.; Garcia, G. E.; Geissler, P. L. Membrane hydrophobicity determines the activation free energy of passive lipid transport. *Biophysical journal* **2021**, *120*, 3718–3731.

(69) Vermaas, J. V.; Beckham, G. T.; Crowley, M. F. Membrane permeability of fatty acyl compounds studied via molecular simulation. *The Journal of Physical Chemistry B* **2017**, *121*, 11311–11324.

(70) Sindhikara, D. J.; Emerson, D. J.; Roitberg, A. E. Exchange often and properly in replica exchange molecular dynamics. *Journal of Chemical Theory and Computation* **2010**, *6*, 2804–2808.

(71) Vermaas, J. V.; Bentley, G. J.; Beckham, G. T.; Crowley, M. F. Membrane permeability of terpenoids explored with molecular simulation. *The Journal of Physical Chemistry B* **2018**, *122*, 10349–10361.

(72) Harris, C. R. et al. Array programming with NumPy. *Nature* **2020**, *585*, 357–362.

(73) Hunter, J. D. Matplotlib: A 2D graphics environment. *Computing in science & engineering* **2007**, *9*, 90–95.

(74) Diamond, J. M.; Katz, Y. Interpretation of nonelectrolyte partition coefficients between dimyristoyl lecithin and water. *The Journal of membrane biology* **1974**, *17*, 121–154.

(75) Bennion, B. J.; Be, N. A.; McNerney, M. W.; Lao, V.; Carlson, E. M.; Valdez, C. A.; Malfatti, M. A.; Enright, H. A.; Nguyen, T. H.; Lightstone, F. C.; others Predicting a drug's membrane permeability: A computational model validated with in vitro permeability assay data. *The journal of physical chemistry B* **2017**, *121*, 5228–5237.

(76) Vermaas, J. V.; Dixon, R. A.; Chen, F.; Mansfield, S. D.; Boerjan, W.; Ralph, J.; Crowley, M. F.; Beckham, G. T. Passive membrane transport of lignin-related compounds. *Proceedings of the National Academy of Sciences* **2019**, *116*, 23117–23123.

(77) Ferguson, A. L. BayesWHAM: A Bayesian approach for free energy estimation, reweighting, and uncertainty quantification in the weighted histogram analysis method. *Journal of Computational Chemistry* **2017**, *38*, 1583–1605.

(78) Habeck, M. Bayesian estimation of free energies from equilibrium simulations. *Physical Review Letters* **2012**, *109*, 100601.

(79) Hummer, G. Position-dependent diffusion coefficients and free energies from Bayesian analysis of equilibrium and replica molecular dynamics simulations. *New Journal of Physics* **2005**, *7*, 34.

(80) Gaalswyk, K.; Awoonor-Williams, E.; Rowley, C. N. Generalized Langevin methods for calculating transmembrane diffusivity. *Journal of Chemical Theory and Computation* **2016**, *12*, 5609–5619.

(81) Fujimoto, K.; Nagai, T.; Yamaguchi, T. Momentum removal to obtain the position-dependent diffusion constant in constrained molecular dynamics simulation. *Journal of Computational Chemistry* **2021**, *42*, 2136–2144.

(82) Vermaas, J. V.; Crowley, M. F.; Beckham, G. T. Molecular simulation of lignin-related aromatic compound permeation through gram-negative bacterial outer membranes. *Journal of Biological Chemistry* **2022**, 102627.

(83) Galassi, V. V.; Arantes, G. M. Partition, orientation and mobility of ubiquinones in a lipid bilayer. *Biochimica et Biophysica Acta (BBA)-Bioenergetics* **2015**, *1847*, 1560–1573.

(84) Singharoy, A.; Maffeo, C.; Delgado-Magnero, K. H.; Swainsbury, D. J.; Sener, M.; Kleinekathöfer, U.; Vant, J. W.; Nguyen, J.; Hitchcock, A.; Isralewitz, B.; others Atoms to phenotypes: molecular design principles of cellular energy metabolism. *Cell* **2019**, *179*, 1098–1111.

(85) Neale, C.; Pomès, R. Sampling errors in free energy simulations of small molecules in lipid bilayers. *Biochimica et Biophysica Acta (BBA)-Biomembranes* **2016**, *1858*, 2539–2548.

(86) Tieleman, D. P.; Marrink, S.-J. Lipids out of equilibrium: Energetics of desorption and pore mediated flip-flop. *Journal of the American Chemical Society* **2006**, *128*, 12462–12467.

(87) Ferrell Jr, J. E.; Lee, K. J.; Huestis, W. H. Lipid transfer between phosphatidylcholine vesicles and human erythrocytes: exponential decrease in rate with increasing acyl chain length. *Biochemistry* **1985**, *24*, 2857–2864.

(88) Nichols, J. W. Thermodynamics and kinetics of phospholipid monomer-vesicle interaction. *Biochemistry* **1985**, *24*, 6390–6398.

(89) Raza, S.; Sievertsen, T. H.; Okumoto, S.; Vermaas, J. V. Passive permeability controls synthesis for the allelochemical sorgoleone in sorghum root exudate. 2023; `https://doi.org/10.5281/zenodo.8212450`.

(90) Towns, J.; Cockerill, T.; Dahan, M.; Foster, I.; Gaither, K.; Grimshaw, A.; Hazlewood, V.; Lathrop, S.; Lifka, D.; Peterson, G. D.; Roskies, R.; Scott, J. R.; Wilkens-Diehr, N. XSEDE: Accelerating Scientific Discovery. *Comput. Sci. Eng.* **2014**, *16*, 62–74.